NUCL SCI TECH (2021) 32:19
https://doi.org/10.1007/s41365-021-00853-7

Probing granular inhomogeneity of a particle-emitting source by imaging two-pion Bose–Einstein correlations

Li-Ya Li[1] · Peng Ru[2] · Ying Hu[1]

Received: 30 August 2020 / Revised: 8 December 2020 / Accepted: 10 December 2020 / Published online: 19 February 2021

Abstract Using the source imaging technique in two-pion interferometry, we study the image of the hydrodynamic particle-emitting source with the HIJING initial conditions for relativistic heavy-ion collisions on an event-by-event basis. It is shown that the initial-state fluctuations may give rise to bumpy structures of the medium during hydrodynamical evolution, which affects the two-pion emission space and leads to a visible two-tiered shape in the source function imaged using the two-pion Bose–Einstein correlations. This two-tiered shape can be understood within a similar but more analytic granular source model and is found to be closely related to the introduced quantity ξ, which characterizes the granular inhomogeneity of the source. By fitting the imaged source function with a granular source parametrization, we extract the granular inhomogeneity of the hydrodynamic source, which is found to be sensitive to both the Gaussian smearing width of the HIJING initial condition and the centrality of the collisions.

This work was supported in part by the Research Start-up Funding of Hubei University of Education (No. 201801), Hubei Provincial Natural Science Foundation of China (No. 2020CFB697), the China Postdoctoral Science Foundation (No. 2019M652929), the MOE Key Laboratory of Quark and Lepton Physics (Central China Normal University) (No. QLPL201802).

✉ Ying Hu
yinghu@hust.edu.cn

[1] School of Mathematics and Economics, Hubei University of Education, Wuhan 430205, Hubei, China

[2] Guangdong Provincial Key Laboratory of Nuclear Science, Institute of Quantum Matter, South China Normal University, Guangzhou 510006, China

Keywords Heavy-ion collision · Bose–Einstein correlations · Imaging technique

1 Introduction

In relativistic heavy-ion collisions, the properties and evolution dynamics of the created QCD matter in different stages of the collisions are encoded in various final-state observables. The Hanbury Brown–Twiss correlation of two final-state particles is one such unique observable that provides a more direct information on the space-time geometry of the particle-emitting source [1–5]. In particular, with the development of the source imaging techniques in pion interferometry [6–8], two-pion Bose–Einstein correlations have been able to serve as a "camera" for the medium [9–11]. This makes it possible to probe the detailed structures of the particle-emitting source with its image and provides a more intuitive understanding of the evolution dynamics of the medium.

For an event of heavy-ion collisions, the spatial distribution of the medium is usually not smooth, because of initial-state fluctuations [12–14], and there may be some hot spots and cold valleys distributed in the medium. In Ref. [15], it was found that a source with a granular structure has a very different imaging effect from that of a Gaussian source, for example, the imaged source function has a prominent two-tiered shape. Thus, it will be interesting to study a source with a more general particle-emitting source model to determine whether the bumpy spatial distribution of the medium can result in any similar signal in the source image and to examine how the detailed source structures affect the image.

In this work, we utilize the source imaging technique in two-pion interferometry to study the image of the hydrodynamic particle-emitting source with the initial conditions fluctuating from event to event. The evolution of the medium is simulated with a (2+1)-dimensional ideal hydrodynamic code [16], and the initial conditions are generated using the Heavy Ion Jet Interaction Generator (HIJING) [17, 18]. It was found that the imaged source function of the hydrodynamic source can exhibit a non-Gaussian twofold(two-tiered) shape. This two-tiered structure can be understood by introducing a simpler granular source model and is characterized by the granular inhomogeneity ξ by means of a granular source. By fitting the imaged source function with a granular source parametrization, we extract the granular inhomogeneity of the hydrodynamic source, which is found to be sensitive to both the Gaussian smearing width of the HIJING initial condition and the centrality of the collisions.

The rest of this paper is organized as follows. In Sect. 2, we model the space-time evolution of the hydrodynamic source with the HIJING initial conditions. In Sect. 3, we study the imaging of the hydrodynamic source. In Sect. 4, we extract the granular inhomogeneity of the hydrodynamic source by fitting the source function with a granular source parametrization. Finally, we give a summary and discussion in Sect. 5.

2 Hydrodynamically evolving sources with fluctuating initial conditions from HIJING

As a particle-emitting source, the fireball created in an event of heavy-ion collisions is likely to be spatially bumpy because of initial-state fluctuations and a subsequent evolution period with a nearly perfect fluidity [19]. In this work, we perform (2+1)-dimensional hydrodynamic simulations for the evolution of the bulk medium on an event-by-event basis. The framework of our simulation has been applied in Ref. [16] and was shown to be able to well describe the experimental data on the pion transverse momentum spectrum.

To take into account the initial-state fluctuations, we utilize the HIJING event generator [17, 18] to construct the initial energy density profile at a hydrodynamic starting time τ_0 and at the space-time rapidity $\eta_S = 0$, which is written by summing over the contributions of the produced minijet partons as [13, 20, 21]

$$\varepsilon(\tau_0, x, y\,; \eta_S = 0) = K \sum_\alpha \frac{p_{\perp\alpha}}{\tau_0} \frac{1}{2\pi\sigma_\perp^2} \times \exp\left\{ -\frac{[x - x_\alpha(\tau_0)]^2 + [y - y_\alpha(\tau_0)]^2}{2\sigma_\perp^2} \right\}, \tag{1}$$

where $p_{\perp\alpha}$ is the transverse momentum of parton α, $x_\alpha(\tau_0)$ and $y_\alpha(\tau_0)$ are the transverse coordinates of the parton at τ_0, $\sigma_\perp$ is the transverse width parameter of the Gaussian smearing, and K is a scale factor that contains the parton rapidity normalization coefficient and can be adjusted to fit the experimental data for final-state hadrons. In this study, we consider $K = 0.2$ for the LHC energy by fitting the pion transverse momentum spectrum at central rapidity [22]. The initial condition at any space-time rapidity η_S can be obtained using the longitudinal boost invariance hypothesis.

To visualize the geometric structure of the medium initial profile, in Fig. 1, we demonstrate the transverse distributions of the energy density at $\tau_0 = 0.4$ fm$/c$ for two representative events of Pb+Pb collisions at $\sqrt{s_{\mathrm{NN}}} = 2.76$ TeV, with the impact parameters $b = 0$ fm [panels (a) and (b)] and $b = 6$ fm [panels (c) and (d)], respectively. Since the Gaussian smearing width $\sigma_\perp$, related to the energy depositions of the produced partons, can affect the geometric structure of the medium, we compare the initial profiles constructed with $\sigma_\perp = 0.4$ fm [panels (a) and (c)] to those constructed with $\sigma_\perp = 0.8$ fm [panels (b) and (d)] for each studied impact parameter in Fig. 1.

One can observe from Fig. 1 that the transverse profile of the HIJING initial condition can exhibit a bumpy structure with some hot spots and cold valleys. The number of the hot spots (or cold valleys) in a central collision is likely to be greater than that in a peripheral one because of the larger nuclear overlap zone and the greater number of participants. For a given impact parameter, the constructed initial profile with a smaller Gaussian smearing width $\sigma_\perp$ may have more and sharper hot spots, because of the less spreads and overlaps of the deposed energies of the produced partons.

The succeeding evolution of the medium is simulated with a (2+1)-dimensional ideal hydrodynamics program developed earlier [16], which numerically solves the hydrodynamics equations by using the relativistic Harten-Lax-Leer-Einfeldt (RHLLE) algorithm [23]. In our calculation, the parameterized equation of state s95p-PCE [24] is used to close the hydrodynamic equations.

To display the evolution of the medium geometric structure, we record the energy density distributions of the evolving media with the four initial conditions shown in Fig. 1 at the longitudinal proper times τ =3, 6, and 9 fm$/c$ and are shown in Fig. 2. It is observed from Fig. 2 that an initial bumpy structure of the fluid can give rise to bumpy structures to some extent during the following hydrodynamical evolution. The initial conditions constructed with different Gaussian smearing widths $\sigma_\perp$ can result in visible

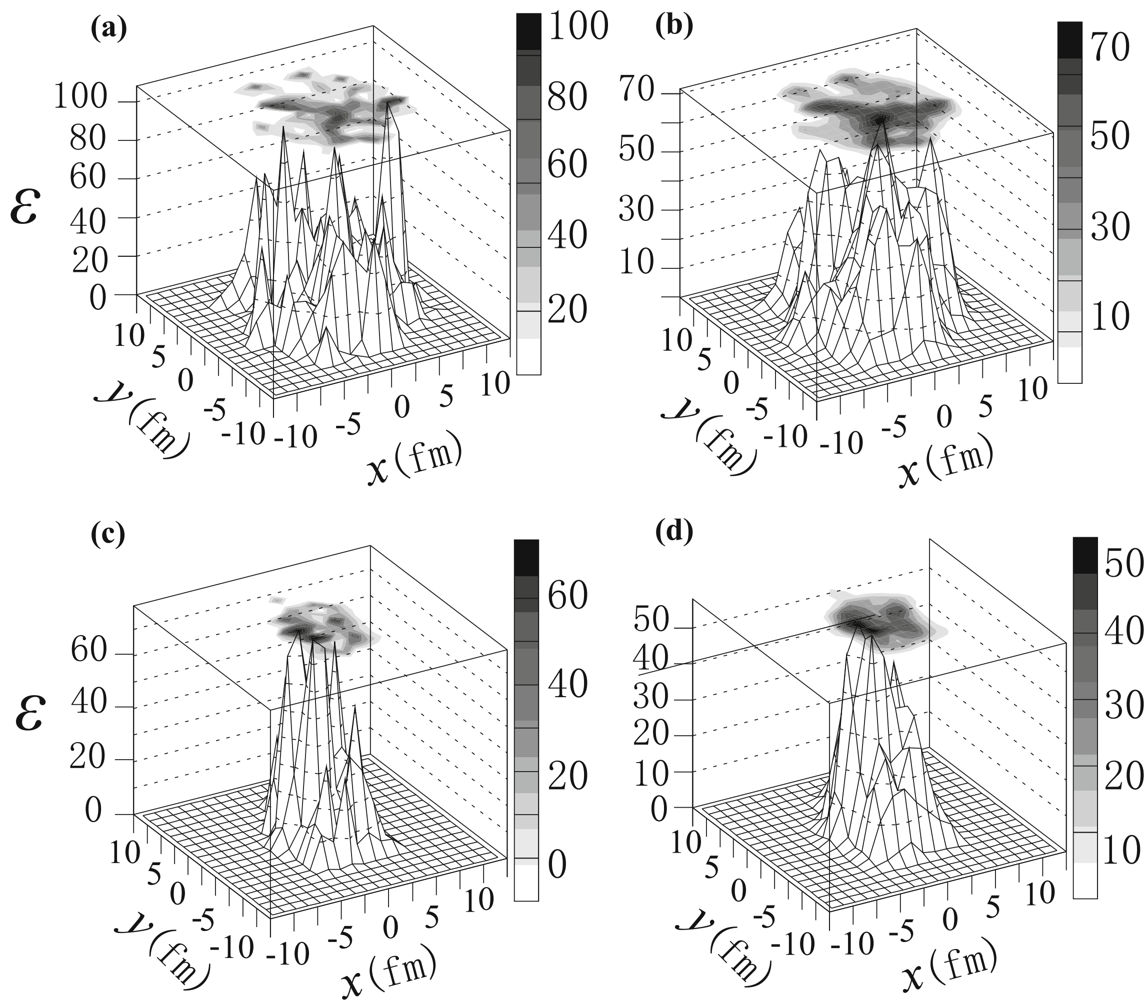

Fig. 1 (Color online) Initial transverse distributions of energy density ($\tau_0 = 0.4$ fm$/c$) constructed with the HIJING generator for Pb+Pb collisions at $\sqrt{s_{\mathrm{NN}}} = 2.76$ TeV. Panels **a**, **b** depict the initial profiles for an event with the impact parameter $b = 0$ fm, constructed with $\sigma_\perp = 0.4$ fm and 0.8 fm, respectively. Panels **c**, **d** depict those for an event with $b = 6$ fm. Unit of energy density is GeV/fm^3

differences in the succeeding medium structure, even at a later stage of the evolution, for example, at $\tau = 9\,\mathrm{fm}/c$.

In the remainder of this paper, we will introduce a granular inhomogeneity to characterize the medium bumpy structure with hot spots and cold valleys. In general, the detailed structures of the particle-emitting source may have some effects in final-state observables, among which the Bose–Einstein correlations of the identical pions are a much relevant type. Next, we shall study the granular inhomogeneity of the source with the two-pion correlations and the related source imaging technique.

3 Imaging of hydrodynamical source with the HIJING initial condition

The basic idea of the imaging technique [6, 7, 25] in pion interferometry is to extract the two-pion source function $S(\mathbf{r})$ from the two-pion Bose–Einstein correlation function $C(\mathbf{q})$. This is usually achieved by noting that $C(\mathbf{q})$ can be expressed in the center-of-mass (c.m.) frame of the pion pair, with the Koonin–Pratt equation [26, 27],

$$C(\mathbf{q}) - 1 = \int \mathrm{d}\mathbf{r} K(\mathbf{q}, \mathbf{r}) S(\mathbf{r}), \tag{2}$$

where $\mathbf{q} = \mathbf{p}_1 - \mathbf{p}_2$ is the relative momentum of the pion pair, and $K(\mathbf{q}, \mathbf{r}) = |\Phi_{\mathbf{q}}(\mathbf{r})|^2 - 1$ is the kernel of the integral equation, with $\Phi_{\mathbf{q}}(\mathbf{r})$ being the wave function related to the propagation of the pion pair emitted from a relative separation of $\mathbf{r}$ in the pair c.m. frame. In the absence of the

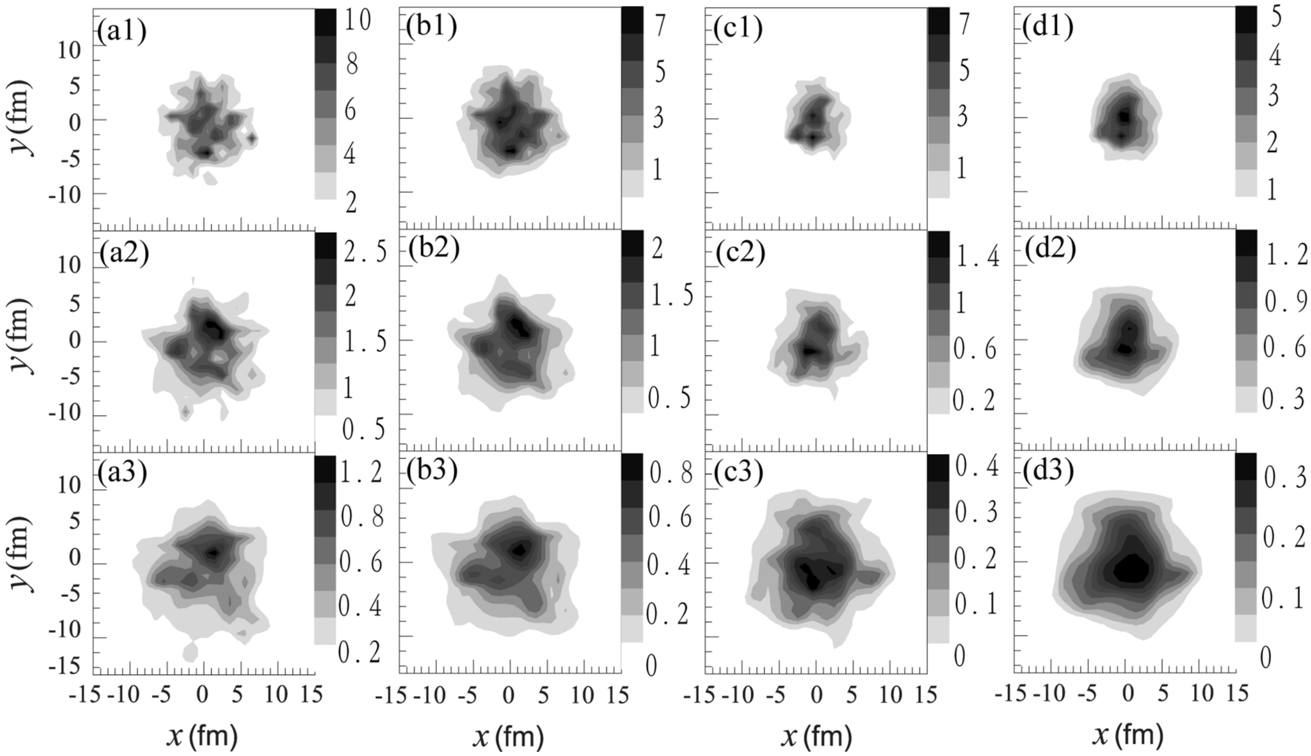

Fig. 2 (Color online) Transverse distributions of the energy density of four evolving systems recorded at $\tau = 3$ fm$/c$ (**a1–d1**), $\tau = 6$ fm$/c$ (**a2–d2**), and $\tau = 9$ fm$/c$ (**a3–d3**). The corresponding initial conditions for these four systems are shown in Fig. 1(a–d), respectively. The unit of energy density is GeV/fm^3

final-state interaction of the pion pair, the wave function $\Phi_{\mathbf{q}}(\mathbf{r}) = (e^{i\mathbf{q}\cdot\mathbf{r}/2} + e^{-i\mathbf{q}\cdot\mathbf{r}/2})/\sqrt{2}$ and the two-pion correlation are entirely induced by Bose–Einstein symmetrization.

The source function $S(\mathbf{r})$ can be interpreted as the quasi-probability for the source to emit a pion pair with a relative separation of $\mathbf{r}$ in the pair c.m. frame. It can be written as the convolution of the normalized single-particle emission function $D(\mathbf{r}, t, \mathbf{p})$ [25, 28],

$$S(\mathbf{r}) = \int \mathrm{d}t \int \mathrm{d}^3R\, \mathrm{d}T D(\mathbf{R} + \mathbf{r}/2, T + t/2, \mathbf{p}_1) \times D(\mathbf{R} - \mathbf{r}/2, T - t/2, \mathbf{p}_2). \tag{3}$$

In general, for an evolving particle-emitting source, the source function $S(\mathbf{r})$ is related to the time-averaged geometry of the two-pion emission space.

To extract the image of the source, that is, the source function $S(\mathbf{r})$ from $C(\mathbf{q})$, one needs to invert Eq. (2). The 3D problem is usually reduced to a 1D radial one by performing the angle average of Eq. (2). The angle-averaged version of Eq. (2) [15, 28]

$$\mathcal{R}(q_{\mathrm{inv}}) \equiv C(q_{\mathrm{inv}}) - 1 = \int \mathrm{d}r\, r^2 K(q_{\mathrm{inv}}, r) S(r), \tag{4}$$

where $q_{\mathrm{inv}} = \sqrt{\mathbf{q}^2 - q_0^2}$ and $K(q_{\mathrm{inv}}, r) = \sin(q_{\mathrm{inv}} r)/(q_{\mathrm{inv}} r)$ with the final-state interaction being neglected. In this work, we solve the problem of inverting Eq. (4) by using the method discussed in Refs. [15, 28].

Next, we study the imaging of the hydrodynamically evolving source with fluctuating initial conditions (FIC) from HIJING on an event-by-event basis. In our model calculations, we simulate 100 events for a given impact parameter and sample 10^4 pion pairs for each event to evaluate the correlation function $C(q_{\mathrm{inv}})$. The pions are emitted thermally from the sources at a freeze-out temperature $T_f = 150$ MeV. We choose the pion pairs in the transverse momentum range $0.2 \le K_T \le 0.6$ GeV$/c$ for the calculations.

In panel (a) of Fig. 3, we show the event-averaged two-pion correlation function $C(q_{\mathrm{inv}})$ for Pb+Pb collisions at $\sqrt{s_{\mathrm{NN}}} = 2.76$ TeV with the impact parameter $b = 0$ fm. Here, the Gaussian smearing width for the HIJING initial condition is taken to be $\sigma_\perp = 0.4$ fm. The extracted source function is shown with black circles in panel (c) of Fig. 3. For comparison, the correlation function for a Gaussian source with radius $R_{\mathrm{ga}} = 6.0$ fm is plotted in panel (b) of Fig. 3, and the corresponding imaged source function is shown with black circles in panel (d). It can be observed that the image of the Gaussian source has a simple

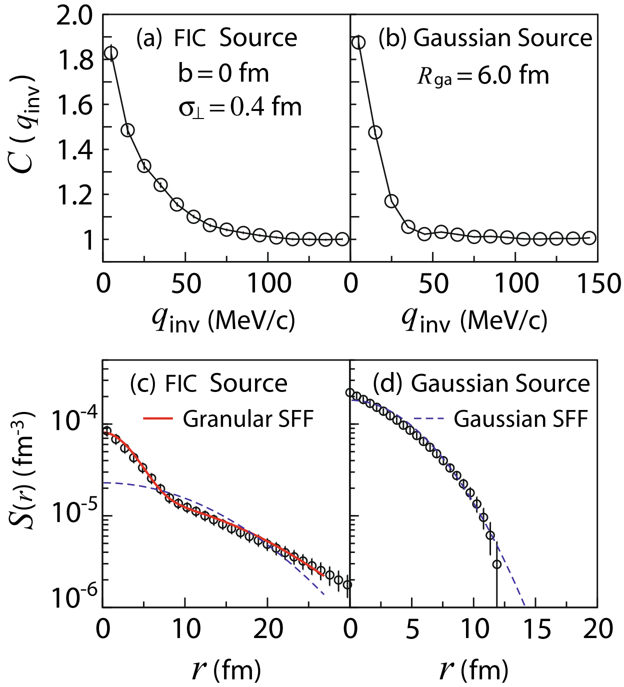

Fig. 3 (Color online) Panels **a**, **b** Two-pion correlation functions for FIC and Gaussian sources, respectively. Panels **c**, **d** Source functions for FIC and Gaussian sources, respectively. In panels **c**, **d**, black circles represent the results extracted by the imaging technique, the black dash curve represents Gaussian source function fitting (SFF), and the red solid curve represents granular SFF

structure, whereas that of the hydrodynamic source with FIC from HIJING exhibits a twofold (or two-tiered) structure. We shall try to understand this difference in an analytical way.

For a Gaussian source, the source function can be written as [28],

$$S^{\mathrm{Ga}}(r)=\frac{1}{(\sqrt{4\pi}R_{\mathrm{ga}})^3}\ \exp\left(-\frac{r^2}{4R_{\mathrm{ga}}^2}\right). \tag{5}$$

With this function, we fit the imaged sources in panels (c) and (d) of Fig. 3. The Gaussian source function fitting (SFF) is in good agreement with the image of the Gaussian source extracted from the correlation function, as expected. However, the Gaussian SFF can hardly describe the image of the hydrodynamic source with FIC ($\chi^2/\mathrm{NDF}=5.96$).

The two-tiered structure of the image of the hydrodynamic source with FIC is possibly related to the bumpy structure of the source with hot spots and cold valleys. To analytically demonstrate this, we consider a simpler static granular source model [15, 29, 30] in which the particles are emitted from dispersed droplets, and each individual droplet is assumed to be a Gaussian emission source. The source function for the granular source model can be written as [15]

$$S(\mathbf{r})=\frac{1}{N^2(\sqrt{4\pi}a)^3}\sum_{i,j=1}^{N}\exp\left[-\frac{(\mathbf{r}-\mathbf{X}_{ij})^2}{4a^2}\right]. \tag{6}$$

where a is the radius of the droplets, $\mathbf{X}_{ij}$ is the spatial separation between the centers of the ith and jth droplets, and N is the number of droplets in the granular source. Assuming that the coordinates of the droplet centers, $\mathbf{X}_i$, are distributed in a Gaussian form, i.e., $P(\mathbf{X}_i)\sim\exp(-\mathbf{X}_i^2/2R_{\mathrm{gr}}^2)$, the event-averaged source function (extracted from the event-averaged correlation function) of the granular source reads [15, 30]

$$S^{\mathrm{Gr}}(r)=\frac{1}{N}\frac{1}{(\sqrt{4\pi}a)^3}\ \exp\left(-\frac{r^2}{4a^2}\right)+\left(1-\frac{1}{N}\right)\times\frac{1}{(\sqrt{4\pi}\sqrt{a^2+R_{\mathrm{gr}}^2})^3}\exp\left[-\frac{r^2}{4(a^2+R_{\mathrm{gr}}^2)}\right]. \tag{7}$$

The spatial structure of the granular source is somewhat similar to that of the bumpy hydrodynamic source with hot spots and cold valleys (for example, the droplet in the granular source is similar to the hot spot in the hydrodynamic source). Obviously, the source function of the granular source involves two exponential terms associated with two scales, that is, a and $(a^2+R_{\mathrm{gr}}^2)^{1/2}$, respectively. The two terms correspond to the cases where the two pions are emitted from the same droplet and from different droplets, respectively.

Using the parameterized function in Eq. (7), we do the source function fitting for the hydrodynamic source with FIC (details of the fitting can be seen in Sect. 4) and demonstrate the result as the red solid curve in panel (c) of Fig. 3. It is interesting to see that the granular SFF can well describe the image of the hydrodynamic source with FIC from HIJING ($\chi^2/\mathrm{NDF}=0.14$). We expect that Eq. (7) can provide some intuitions for understanding the geometric structure of the hydrodynamic source.

From Eq. (7), we can find that the shape of the two-tiered source function is sensitive to the source geometry. For $R_{\mathrm{gr}}^2\gg a^2$, that is, the size of the whole source is much larger than that of the inside droplets, the ratio of the coefficients of the two terms in Eq. (7) is approximated as $(R_{\mathrm{gr}}/a)^3/(N-1)$, which is a characteristic quantity for the two-tiered source function. Assuming that $N\geq 2$ can be considered in the sense of a granular source, we can use a quantity [15]

$$\xi=\frac{(R_{\mathrm{gr}}/a)^3}{N-2}, \tag{8}$$

to characterize the source geometric feature that gives rise to the two-tiered structure of the source function. We will refer to this feature as the granular inhomogeneity of the source in this work. It is also noteworthy that the quantity ξ is closely related to the averaged packing fraction $p \equiv N(a/R_{\rm gr})^3$ in the sense of the granular source, with the relation $\xi = \frac{N}{(N-2)} p^{-1}$.

For the granular source, the quantity ξ or the granular inhomogeneity will increase with the increasing radius of the whole source ($R_{\rm gr}$), but decrease with both the increasing radius of the inside droplet (a) and the increasing number of droplets (N). Figure 4 illustrates the source functions in Eq. (7) with different values of the parameters (and granular inhomogeneity ξ). We can find that the two-tiered structure of the source functions is sensitive to the value of ξ and becomes more significant for a larger ξ. The two-tiered shape will degenerate into a Gaussian shape in the limit $\xi \to 0$.

4 Extracting granular inhomogeneity of hydrodynamic source from source image

The source function $S^{\rm Gr}(r)$ of the granular source given in Eq. (7) can serve as a useful parametrization to study and quantify the granular inhomogeneity (ξ) for a more general particle-emitting source, through fitting the source function imaged from the two-pion Bose–Einstein correlation functions. In this section, we shall study the granular inhomogeneity of the hydrodynamic source with fluctuating initial conditions from HIJING.

In Fig. 5, we illustrate the event-averaged images of the hydrodynamic sources with the HIJING initial conditions (black circles). The simulation is performed for the Pb+Pb collisions at $\sqrt{s_{\rm NN}} = 2.76$ TeV, with impact parameters $b = 0$ fm and $b = 6$ fm. The Gaussian smearing width $\sigma_\perp$ for the initial condition is taken to be 0.4 fm and 0.8 fm. (For representative events and corresponding evolutions, see Figs. 1 and 2.) We can observe that all the source images in Fig. 5 exhibit a two-tiered structure.

In order to extract the source granular inhomogeneity from the source image $S(r)$, we perform the source function fitting with the parametrization $\lambda S^{\rm Gr}(r)$, in which $S^{\rm Gr}(r)$ is in the form of Eq. (7), and λ is the strength factor of the correlation function. Concretely, we have preset the values of the positive integers N and considered λ, a, and $R_{\rm gr}$ as free parameters in the fitting. This procedure will be performed for different N values until the minimum $\chi^2/{\rm NDF} < 1$ is met. The results of the fitting are shown in Fig. 5 as red curves. It is observed that the parametrization $\lambda S^{\rm Gr}(r)$ can describe the images of the hydrodynamic sources fairly well.

In Table 1, we list the extracted parameters in the fitting as well as the corresponding minimum $\chi^2/{\rm NDF}$. The extracted granular inhomogeneity ξ is found to be sensitive to the Gaussian smearing width $\sigma_\perp$ in the initial condition.

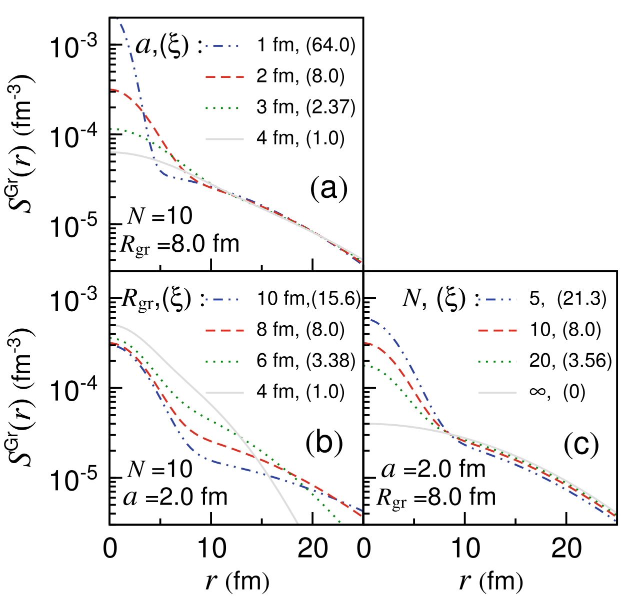

Fig. 4 (Color online) Source functions for static granular sources with different values of source parameters. In panel **a**, we consider $N = 10$ and $R_{\rm gr} = 8.0$ fm and vary the parameter a. In panel **b**, we consider $N = 10$ and $a = 2.0$ fm and vary the parameter $R_{\rm gr}$. In panel **c**, we take $a = 2.0$ fm and $R_{\rm gr} = 8.0$ fm and vary the parameter N. The corresponding values of ξ are also shown

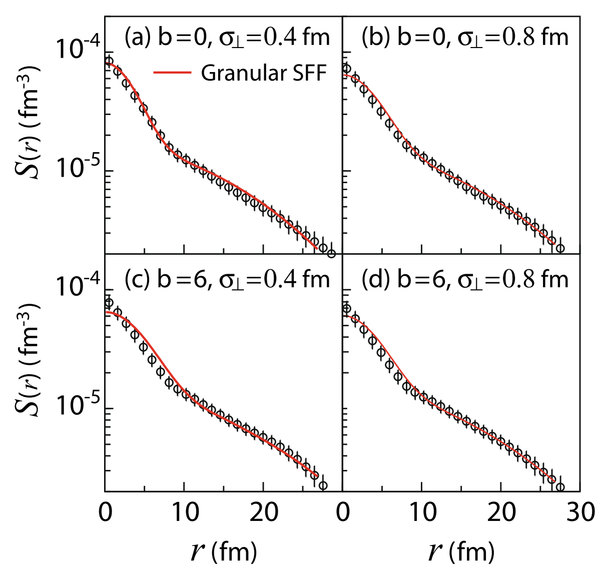

Fig. 5 (Color online) Event-averaged source function imaging for a hydrodynamic source with the HIJING initial condition (black circles). Simulation is performed for Pb+Pb collisions at $\sqrt{s_{\rm NN}} = 2.76$ TeV, with the impact parameters $b = 0$ fm (panels **a**, **b**) and $b = 6$ fm (panels **c**, **d**). The Gaussian smearing width $\sigma_\perp$ for the initial condition is considered to be 0.4 fm (panels **a**, **c**) and 0.8 fm (panels **b**, **d**). The red curve represents the result of source function fitting with parametrization $S^{\rm Gr}(r)$ in Eq. (7)

Table 1 Parameters related to source granular inhomogeneity, extracted by fitting the imaged hydrodynamics source function with granular source parametrization in Eq. (7)

	(a) $b = 0$ fm $\sigma_\perp = 0.4$ fm	(b) $b = 0$ fm $\sigma_\perp = 0.8$ fm	(c) $b = 6$ fm $\sigma_\perp = 0.4$ fm	(d) $b = 6$ fm $\sigma_\perp = 0.8$ fm
R_{gr} (fm)	9.32 ± 0.30	9.69 ± 0.35	8.24 ± 0.37	8.69 ± 0.66
a (fm)	2.23 ± 0.06	2.74 ± 0.09	3.30 ± 0.11	4.76 ± 0.21
λ	0.65 ± 0.03	0.69 ± 0.04	0.77 ± 0.04	0.78 ± 0.06
N(fixed)	20	15	10	6
χ^2/NDF	0.17	0.16	0.57	0.68
ξ	4.05 ± 0.65	3.40 ± 0.61	1.95 ± 0.37	1.52 ± 0.37

The corresponding minimum χ^2/NDF are also shown

For a given impact parameter, ξ is larger for a smaller $\sigma_\perp$, mainly due to the smaller a (droplet radius parameter) extracted in the fitting, which may indicate that the average radius of the hot spots in the evolving medium is smaller for a smaller $\sigma_\perp$. The reduction in the droplet number N for a larger $\sigma_\perp$ may imply an enhanced hot spot merging effect. Moreover, the extracted granular inhomogeneity ξ in central collisions is larger than that in the peripheral ones. On the one hand, because the averaged radius of the whole source is larger in central collisions, the extracted R_{gr} is larger. On the other hand, the extracted a is smaller in central collisions, which also results in a larger ξ and indicates that the average radius of the medium hot spots during the hydrodynamic evolution may be smaller in more central collisions. This may also be related to the fact that the droplet number N is not treated as a free parameter in the fitting, which should be examined in a future study.

The results in this work indicate that the source image, extracted from the two-pion Bose–Einstein correlations, may provide valuable information on the granular inhomogeneity of the particle-emitting source, which may be sensitive to both the source initial condition and the source dynamical evolution.

5 Summary and discussion

In this work, we utilize the final-state two-pion Bose–Einstein correlations to study the imaging of the hydrodynamic particle-emitting source with the initial conditions fluctuating from event to event. The evolution of the medium is simulated with a (2+1)-dimensional ideal hydrodynamic code, and the initial conditions are generated with HIJING. It is shown that initial-state fluctuations can give rise to bumpy structures of the medium to some extent during the succeeding hydrodynamical evolution, which is sensitive to the Gaussian smearing width of the parton energy deposition in the initial condition.

It is found that the imaged source function of the hydrodynamic source can exhibit a non-Gaussian twofold (two-tiered) shape. This is mainly due to the bumpy structure of the medium with hot spots and cold valleys, which affects the two-pion emission space. The two-tiered structure of the source function can be partly explained by introducing a simpler granular source model that can be solved analytically and can be characterized by the granular inhomogeneity ξ by means of a granular source.

The parametrization form of the granular source function is found to be able to describe the image of the hydrodynamic source with the HIJING initial conditions. By fitting the source image with the granular source function parametrization, we extract the granular inhomogeneity ξ of the hydrodynamic source. We find that the extracted ξ is sensitive to the Gaussian smearing width of the HIJING initial condition, as well as the centrality of the collisions.

In this work, the medium evolution is modeled with ideal hydrodynamics. If the viscosity of the fluid is considered [14, 31, 32], the bumpy structure of the medium may become less important in the middle and later stages of the evolution owing to the dissipation. Thus, it will be interesting to study the effect of viscosity on source imaging and granular inhomogeneity in the future. In addition, the image of the source in this work is extracted from the Bose–Einstein correlations by neglecting the final-state interactions, for example, the Coulomb force and resonance decay. It has been realized that the final-state effects, such as long-lived-resonance emission halo [9, 30, 33], may also give rise to a multifold structure in the source image, which may affect the extraction of the source granular inhomogeneity in experiments. Compared to the effect of the source granular inhomogeneity, that is, an increase in the probability of shorter-distance pion pair emission, the resonance decays are expected to enhance the long-distance pion pair emission and result in a long tail of the imaged source function. To study the source granular inhomogeneity in heavy-ion experiments, we may need to examine the final-state-corrected experimental measurement of the Bose–Einstein correlations [34, 35] or take into account the effects of the final-state interactions in the calculations [36, 37].

Author Contributions All authors contributed to the study conception and design. Material preparation, data collection, and analysis were performed by Li-Ya Li, Peng Ru, and Ying Hu. The first draft of the manuscript was written by Ying Hu, and all authors commented on previous versions of the manuscript. All authors read and approved the final manuscript.

References

1. U.A. Wiedemann, U. Heinz, Particle interferometry for relativistic heavy ion collisions. Phys. Rep. **319**, 145 (1999). https://doi.org/10.1016/S0370-1573(99)00032-0
2. R.M. Weiner, Boson interferometry in high-energy physics. Phys. Rep. **327**, 249 (2000). https://doi.org/10.1016/S0370-1573(99)00114-3
3. M.A. Lisa, S. Pratt, R. Soltz et al., Femtoscopy in relativistic heavy ion collisions. Ann. Rev. Nucl. Part. Sci. **55**, 357 (2005). https://doi.org/10.1146/annurev.nucl.55.090704.151533
4. A.G. Yang, Y. Zhang, L. Cheng et al., Squeezed back-to-back correlation of D0D0 in relativistic heavy-ion collisions. Chin. Phys. Lett. **35**, 052501 (2018). https://doi.org/10.1088/0256-307X/35/5/052501
5. L. Zhou, D.Q. Fang, Effect of source size and emission time on the pCp momentum correlation function in the two-proton emission process. Nucl. Sci. Tech. **31**, 52 (2020). https://doi.org/10.1007/s41365-020-00759-w
6. D.A. Brown, P. Danielewicz, Imaging of sources in heavy ion reactions. Phys. Lett. B **398**, 252 (1997). https://doi.org/10.1016/S0370-2693(97)00251-7
7. D.A. Brown, A. Enokizono, M. Heffner et al., Imaging three dimensional two-particle correlations for heavy-ion reaction studies. Phys. Rev. C **72**, 054902 (2005). https://doi.org/10.1103/PhysRevC.72.054902
8. Y. Ren, Q. Feng, W.N. Zhang et al., Analysis of the image of pion-emitting sources in the source center-of-mass frame. Eur. Phys. J. A **53**, 163 (2017). https://doi.org/10.1140/epja/i2017-12351-1
9. S.S. Adler et al., [PHENIX Collaboration], Evidence for a long-range component in the pion emission source in Au + Au collisions at $\sqrt{s_{NN}}$ = 200-GeV. Phys. Rev. Lett. **98**, 132301 (2007). https://doi.org/10.1103/PhysRevLett.98.132301
10. S. Afanasiev et al., [PHENIX Collaboration], Source breakup dynamics in Au+Au collisions at $\sqrt{s_{NN}}$ = 200-GeV via three-dimensional two-pion source imaging. Phys. Rev. Lett. **100**, 232301 (2008). https://doi.org/10.1103/PhysRevLett.100.232301
11. C. Alt *et al.* [NA49 Collaboration], Three-dimensional two-pion source image from Pb+Pb Collisions at $\sqrt{s_{NN}}$ = 17.3-GeV: New constraints for source breakup dynamics. Phys. Lett. B **685**, 41 (2010). https://doi.org/10.1016/j.physletb.2010.01.029
12. A. Adare, M. Luzum, H. Petersen, Initial state fluctuations and final state correlations: status and open questions. Phys. Scr. **87**, 048001 (2013). https://doi.org/10.1088/0031-8949/87/04/048001
13. L. Pang, Q. Wang, X.N. Wang, Effects of initial flow velocity fluctuation in event-by-event (3+1)D hydrodynamics. Phys. Rev. C **86**, 024911 (2012). https://doi.org/10.1103/PhysRevC.86.024911
14. C. Gale, S. Jeon, B. Schenke et al., Event-by-event anisotropic flow in heavy-ion collisions from combined Yang-Mills and viscous fluid dynamics. Phys. Rev. Lett. **110**, 012302 (2013). https://doi.org/10.1016/S0370-1573(99)00032-01
15. Z.T. Yang, W.N. Zhang, L. Huo et al., Imaging of granular sources in high energy heavy ion collisions. J. Phys. G **36**, 015113 (2009). https://doi.org/10.1016/S0370-1573(99)00032-02
16. Y. Hu, W.N. Zhang, Y.Y. Ren, Fluctuations in pion elliptic flow, triangular flow, and HBT correlation functions in ultrarelativistic heavy-ion collisions. J. Phys. G **42**, 045105 (2015). https://doi.org/10.1016/S0370-1573(99)00032-03
17. X.N. Wang, M. Gyulassy, HIJING: a Monte Carlo model for multiple jet production in p p, p A, and A collisions. Phys. Rev. D **44**, 3501 (1991). https://doi.org/10.1103/PhysRevD.44.3501
18. X.N. Wang, pQCD based approach to parton production and equilibration in high-energy nuclear collisions. Phys. Rep. **280**, 287 (1997). https://doi.org/10.1016/S0370-1573(96)00022-1
19. H. Song, S.A. Bass, U. Heinz, et al., 200 A GeV Au + Au collisions serve a nearly perfect quark-gluon liquid. Phys. Rev. Lett. **106**, 192301 (2011). Erratum: [Phys. Rev. Lett. **109**, 139904 (2012)]. https://doi.org/10.1103/PhysRevLett.106.192301, https://doi.org/10.1103/PhysRevLett.109.139904
20. M. Gyulassy, D.H. Rischke, B. Zhang, Hot spots and turbulent initial conditions of quark–gluon plasmas in nuclear collisions. Nucl. Phys. A **613**, 397 (1997). https://doi.org/10.1016/S0375-9474(96)00416-2
21. W. Zhao, Y. Zhou, H. Xu et al., Hydrodynamic collectivity in proton Cproton collisions at 13 TeV. Phys. Lett. B **780**, 495 (2018). https://doi.org/10.1016/S0370-1573(99)00032-07
22. R. Preghenella et al., [ALICE Collaboration], Identified-particle production and spectra with the ALICE detector in Pp and Pb C Pb collisions at the LHC. Acta. Phys. Pol. B **43**, 555 (2012). https://doi.org/10.5506/APhysPolB.43.555
23. D.H. Rischke, Fluid dynamics for relativistic nuclear collisions. Lect. Notes Phys. **516**, 21 (1999). https://doi.org/10.1016/S0370-1573(99)00032-08
24. C. Shen, U. Heinz, P. Huovinen et al., Systematic parameter study of hadron spectra and elliptic flow from viscous hydrodynamic simulations of Au + Au collisions at $\sqrt{s_{NN}} = 200$ GeV. Phys. Rev. C **82**, 054904 (2010). https://doi.org/10.1103/PhysRevC.82.054904
25. D.A. Brown, S.Y. Panitkin, G. Bertsch, Extracting particle freezeout densities and entropies from sources imaged in heavy ion reactions. Phys. Rev. C **62**, 014904 (2000). https://doi.org/10.1016/S0370-1573(99)00114-30
26. S. Pratt, T. Csörgo, J. Zimáyi, Detailed predictions for two pion correlations in ultrarelativistic heavy ion collisions. Phys. Rev. C **42**, 2646 (1990). https://doi.org/10.1016/S0370-1573(99)00114-31
27. S.E. Koonin, Proton pictures of high-energy nuclear collisions. Phys. Lett. **70B**, 43 (1977). https://doi.org/10.1016/S0370-1573(99)00114-32
28. D.A. Brown, P. Danielewicz, Observing nongaussian sources in heavy ion reactions. Phys. Rev. C **64**, 014902 (2001). https://doi.org/10.1016/S0370-1573(99)00114-33
29. C.Y. Wong, W.N. Zhang, Signature of granular structures by single-event intensity interferometry. Phys. Rev. C **70**, 064904 (2004). https://doi.org/10.1016/S0370-1573(99)00114-34
30. W.N. Zhang, Z.T. Yang, Y.Y. Ren, Characteristic quantities of pion-emitting sources extracted by model-independent analysis in relativistic heavy-ion collisions. Phys. Rev. C **80**, 044908 (2009). https://doi.org/10.1016/S0370-1573(99)00114-35
31. P. Romatschke, U. Romatschke, Viscosity information from relativistic nuclear collisions: how perfect is the fluid observed at RHIC? Phys. Rev. Lett. **99**, 172301 (2007). https://doi.org/10.1103/PhysRevLett.99.172301
32. H. Song, U. Heinz, Suppression of elliptic flow in a minimally viscous quark-gluon plasma. Phys. Lett. B **658**, 279 (2008). https://doi.org/10.1016/S0370-1573(99)00114-37
33. S. Nickerson, T. Csörgo, D. Kiang, Testing the core halo model on Bose–Einstein correlation functions. Phys. Rev. C **57**, 3251 (1998). https://doi.org/10.1103/PhysRevC.57.3251

34. B.B. Abelev *et al.* [ALICE Collaboration], Two- and three-pion quantum statistics correlations in Pb–Pb collisions at $\sqrt{s_{NN}} =$ 2.76 TeV at the CERN Large Hadron Collider. Phys. Rev. C **89**, 024911 (2014). https://doi.org/10.1103/PhysRevC.89.024911
35. J. Adam et al., [ALICE Collaboration], Multipion Bose–Einstein correlations in pp, p -Pb, and Pb–Pb collisions at energies available at the CERN Large Hadron Collider. Phys. Rev. C **93**, 054908 (2016). https://doi.org/10.1103/PhysRevC.93.054908
36. C. Plumberg, U. Heinz, Hanbury–Brown–Twiss correlation functions and radii from event-by-event hydrodynamics. Phys. Rev. C **98**, 034910 (2018). https://doi.org/10.1103/PhysRevC.98.034910
37. D. Kincses, M.I. Nagy, M. Csand, Coulomb and strong interactions in the final state of HBT correlations for Lévy type source functions. arXiv:1912.01381 [hep-ph]